ACS Photonics

Article

Cite This: ACS Photonics XXXX, XXX, XXX−XXX

pubs.acs.org/journal/apchd5

A Compound Phase-Modulated Beam Splitter to Distinguish Both Spin and Orbital Angular Momentum

Xuesi Zhao, Xue Feng,* Fang Liu, Kaiyu Cui, Wei Zhang, and Yidong Huang

Department of Electronic Engineering, Tsinghua University, Beijing 100084, China

Supporting Information

ABSTRACT: Based on a phase-modulated metallic nanoslit array, an angular momentum (AM) beam splitter has been demonstrated to distinguish both spin and orbital components carried by the light beam. With such a device, the AM modes could be coupled into nondiffracting surface plasmonic beams propagating toward different directions. According to the experimental results, the extinction ratio for spin AM beam splitting is larger than 10 and the spatial interval of adjacent orbital AM modes (with a topological charge interval of 2) is more than 1.1 μm. We believe that such a device would have great potential to achieve a highly compact photonic integrated circuit with the plasmonic beam.

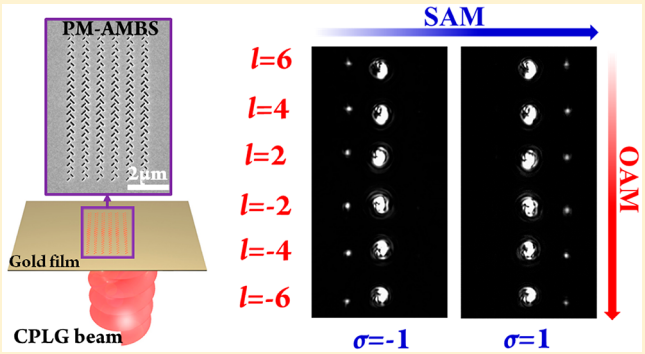

KEYWORDS: *nanoplasmonics, angular momentum of light, nondiffracting surface beam, beam splitter, mode discrimination, metasurfaces, directional coupling*

It is well known that photons can carry both spin and orbital angular momentum (OAM),[1−4] which represent the chirality and helicity of the photon, respectively. The spin angular momentum (SAM) is well known as corresponding to the polarization state of a light beam, while the concept of OAM was relatively unfamiliar until it was found that the Laguerre−Gaussian mode carries well-defined OAM.[5] The OAM, typically operating as an optical vortex with a phase singularity in the center, arises from the helical phase fronts with a form of $\exp(il\varphi)$ where l could be any integer and is known as the topological charge. Vortex beams have been employed in various applications such as optical communication,[6−12] enhanced sensing,[13] imaging,[14,15] quantum procession,[16−18] and light manipulation.[19−23] Especially due to the infinite dimensionality, the OAM is considered as the degree of freedom for high-dimensional information encoding and processing.[9,24,25] On the other hand, SAM is also an important degree of freedom to achieve data processing. To further increase the data capacity, the AM, including both OAM and SAM, have emerged as multiple degrees of freedom for multiplexing encoding in both classical and quantum domains.[9,26,27] Therefore, it is essential to achieve the detection of both OAM and SAM at the terminal of communication systems. Traditional schemes based on bulk components are usually space-consuming and expensive, while devices in practical optical communications are expected to be compact for dense integration.

In recent years, optical metasurfaces have attracted more and more attention since both compact integration and flexibly designing the optical field could be readily achieved.[28−35] Especially, utilizing the surface plasmon polariton (SPP) wave could further reduce the size of devices and achieve nanophotonic circuits within a subwavelength scale, benefiting from the combined confinement of both photons and the collective oscillating electrons.[36−41]

There are some previous works to detect or sort the SAM modes with the help of SPP beams, and the structures include the Λ-shaped metallic nanoslit array[42−47] and metallic nanoslit[46,48] for incidence with phase gradient or geometric phase gradient metasurfaces.[49,50] Those structures could couple the incident light into SPP beams propagating toward different directions according to the carried SAM, respectively. Likewise, several studies on OAM detection have also been conducted. Chen et al.[51] have demonstrated an asymmetric plasmonic nanograting to couple the OAM modes into two separate SPP beams with different splitting angles determined by the topological charges of the incident beams, respectively. The carried OAM could be discriminated by interrogating the splitting angle. However, the generated SPP beam would suffer from beam diffraction, which limits the mode discrimination. To improve it, proper phase modulation could be introduced on the gratings so that the beam diffraction could be controlled. Mei et al.[52] have demonstrated a semiring plasmonic nanoslit to focus the excited SPP beams with reduced beam width in the hot spot to facilitate mode discrimination. However, the spatial interval between adjacent modes is only as small as 120 nm, which is limited by the focal length of the semiring. If the generated SPP beam could propagate without diffraction, the spatial interval would be

Received: October 3, 2019
Published: December 10, 2019

DOI: 10.1021/acsphotonics.9b01437
ACS Photonics XXXX, XXX, XXX−XXX

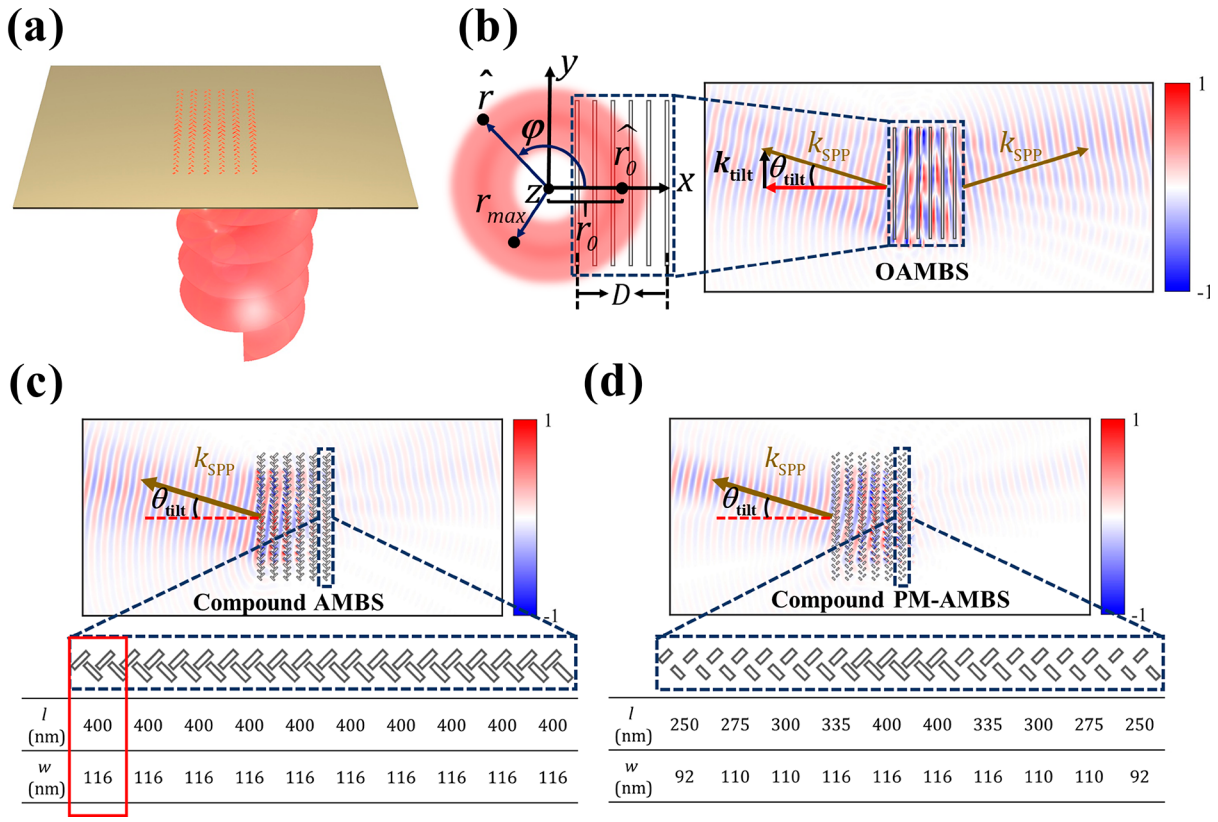

l (nm)	400	400	400	400	400	400	400	400	400	400
w (nm)	116	116	116	116	116	116	116	116	116	116

l (nm)	250	275	300	335	400	400	335	300	275	250
w (nm)	92	110	110	116	116	116	116	110	110	92

Figure 1. (a)Schematics of the AM mode splitting. (b) Schematics of OAM splitting with an OAM beam splitter (OAMBS) with the used parameters and corresponding coordinate also given. (c) Schematics of both SAM and OAM splitting with a compound AM beam splitter (compound AMBS); the corresponding dimension parameters are given in the table below. (d) Schematics of both SAM and OAM splitting with a compound AM beam splitter with phase modulation (compound PM-AMBS) for optimal mode discrimination; the corresponding dimension parameters are given in the table below.

enlarged at a longer distance. Typically, there are several kinds of nondiffracting beams, such as Bessel-like beams,[47,53−61] Airy beams,[45,62−65] bottle beams,[66,67] and arbitrary bending plasmonic beams.[68] Among them, the localized cosine-Gauss beam[47,58−60] (LCGB) is a kind of Bessel-like beam and was first proposed by Lin et al. in 2012. It could propagate along a straight line with most of the energy confined in the main lobe. Therefore, the mode discrimination would be improved if the generated SPP beam is an LCGB. However, there is no report about such a device that could achieve OAM beam splitting, not to mention SAM beam splitting simultaneously.

In this article, a compound phase-modulated angular momentum beam splitter (compound PM-AMBS), which is a combination of grating structure and spatially varied Λ-shaped nanoapertures, is proposed and demonstrated to distinguish both SAM and OAM with optimized mode discrimination. In our previous work,[47] a phase-modulated SAM beam splitter composed of two columns of orthogonally tilted and spatially varied nanoapertures has been demonstrated to separate different SAM modes into unidirectional LCGB propagating toward two opposite sides, respectively. Here, the OAM splitting is also implemented by placing a group of such phase-modulated SAM beam splitters along the azimuth direction of the incident beam profile. The OAM beams would be coupled into LCGBs propagating toward different directions due to their different phase gradients corresponding to the topological charges. With such a compound device, both SAM and OAM beam splitting can be achieved simultaneously. The measured spatial interval for OAM mode splitting is larger than 1.1 μm at the detection position of 30 μm (with topological charge interval of 2), and the extinction ratio for SAM mode splitting is larger than 10.

PRINCIPLE

The incident light beam is considered as a circularly polarized Laguerre−Gaussian (CPLG) beam with a vacuum wavelength of λ. The corresponding complex amplitude of the electric field in the cylindrical coordinate system (r, φ, z) can be written as

$$E(r, \varphi, z) = u_{pl}(\hat{x} \pm i\hat{y}) = u_{pl}e^{\pm i\varphi}(\hat{r} \pm i\hat{\varphi}) = u_{pl}e^{i\sigma\varphi}(\hat{r} + i\sigma\hat{\varphi}) \quad (1)$$

where $\sigma = \pm 1$ denotes the quantized SAM per photon for right/left-handed circular polarization (RHCP/LHCP), respectively, and u_{pl} is the complex amplitude of the Laguerre−Gaussian (LG) mode is and given by

$$u_{pl}(r, \varphi, z) = \frac{a_{pl}}{w(z)}\left(\frac{\sqrt{2}r}{w(z)}\right)^{|l|} L_p^{|l|}\left(\frac{2r^2}{w^2(z)}\right)e^{-r^2/w^2(z)} \times e^{i(\psi - kr^2/2R(z))}e^{-il\varphi} \quad (2)$$

where p is the radial number, l is the topological charge with values of any integer, a_{pl} is the normalized amplitude, $L_p^{|l|}(x)$ is the associated Laguerre polynomial, $w(z)$ is the beam width while $w(0)$ represents the beam waist, and $R(z)$ is the radius of curvature of the wavefront. Furthermore, $\psi = (2p + |l| + 1)\tan^{-1}[z\lambda/\pi w^2(0)]$ is the Gouy phase.

DOI: 10.1021/acsphotonics.9b01437
ACS Photonics XXXX, XXX, XXX−XXX

Here, a CPLG beam carrying both well-defined SAM and OAM is incident from the backside of a metal film and focused on the upper surface. To separate the incident CPLG beams into different directions according to the carried AM (both SAM and OAM), we proposed an on-chip compound phase-modulated AM beam splitter (compound PM-AMBS), which is an array of spatially varied and Λ-shaped metallic nanoapertures as shown in Figure 1a. For the sake of clarity, the operation principle will be discussed in three parts.

OAM Beam Splitter. First, our target is to distinguish OAM carried by a CPLG beam. In the transverse plane (x−y plane) perpendicular to the CPLG beam propagating direction (z-axis), there is an azimuth phase gradient of $k_{OAM} = l/r$, where r is the length of the position vector as shown in Figure 1b. Thus, the topological charge can be identified by measuring such an angular phase gradient. To achieve it, a linear metallic grating coupler with a period (d) of one SPP wavelength (λ_{SPP}) is set along the azimuth direction at a certain position (r, φ) corresponding to the incident beam profile. Actually, the position should only satisfy $r \geq D/2$, where $D = (N-1)d + d_{slit}$ is the width of grating coupler, where N and d_{slit} are the number of slits in the grating and the width of each metallic slit, respectively. However, to achieve higher coupling efficiency, the grating should cover all of the incident CPLG modes with the absolute value of topological charges ranging from $[|l|_{min}, |l|_{max}]$. Therefore, without loss of generality, the grating is set along the y-axis at the position ($r = r_0$, $\varphi = 0$) and $r_0 \approx [r_{max}(|l|_{min}) + r_{max}(|l|_{max})]/2$, where $r_{max}(l) = w(0)\sqrt{2|l|}/2$ is the mode radius with the topological charge l. Besides, $r_{max}(|l|_{min}) - r_{max}(|l|_{max}) \leq D \leq r_{max}(|l|_{min}) + r_{max}(|l|_{max})$ should also be satisfied. The x-coordinate of the ith metallic slit within the grating could be expressed as

$$x_i = r_0 - (N - 2i + 1)d/2,\ i = 1,\ 2,\ \ldots N \tag{3}$$

With such a metallic grating, the incident CPLG beam would be coupled to the SPP mode propagating along the metal surface. Simultaneously, a nearly linear phase gradient $k_{tilt} = k_{OAM}$ ($r = r_{max}$) along the grating coupler is introduced to the SPP beam due to the transverse wave vector matching between the incident CPLG beam and the excited SPP beam. Therefore, a tilt angle of θ_{tilt} would be introduced due to the phase gradient of k_{tilt} and could be expressed as

$$\theta_{tilt} = \arcsin(k_{tilt}/k_{SPP}) \tag{4}$$

where k_{SPP} is the propagation constant of the SPP beam.

Thus, the topological charge of the incident CPLG beam would be mapped to the tilt angle θ_{tilt} of the generated SPP beam. Figure 1b shows the corresponding distribution of the normal electric field, and it can be found that the generated planar SPP beam propagates with a tilt angle of θ_{tilt} in both sides. Therefore, this linear metallic grating coupler acts as an OAM beam splitter (OAMBS), and the incident CPLG beam would be coupled to a certain SPP mode with a tilt angle of θ_{tilt} according to the topological charge of l.

Compound AM Beam Splitter. It should be noted that the OAM beam splitting depends on the position and orientation of the grating rather than the exact type of scattering unit. If each metallic slit in the grating is replaced by another subwavelength scattering unit, the OAM splitting would still be valid. Thus, by properly designing the scattering unit, the SAM mode splitting can be achieved simultaneously. In ref 43, the polarization-controlled directional coupler of the SPP beam is demonstrated, as shown in the dotted box in Figure 1c. Such a coupler consists of two columns of uniform 45° tilted Λ-shaped nanoapertures on the metal film and could split two kinds of SAM modes in two opposite directions. Here, such a coupler is employed to replace the metallic slit in Figure 1b. Therefore, the whole grating composed of several such couplers behaves as a compound AM beam splitter (compound AM-BS) for both SAM and OAM. For the generated SPP beam, the propagation direction (positive/negative x-axis) and the tilt angle θ_{tilt} would be determined by the SAM and OAM carried by the incident CPLG beam. The electric field distribution of the calculated normal component of the generated unidirectional planar SPP beam for the incidence with LHCP is also shown in Figure 1c.

However, the generated SPP beam in either Figure 1b or Figure 1c is a planar wave, which would suffer from beam diffraction. Thus, there would be mode overlap and crosstalk between the two beams with close topological charge.

Compound Phase-Modulated AM Beam Splitter. To further improve the mode discrimination, the excited SPP beam should possess a longer propagation distance and smaller mode volume. In our previous work,[47] we have proposed and demonstrated a phase-modulated coupler, in which a spatially distributed phase gradient of $\varphi(y) = -k_{SPP}|y|\sin(\alpha)$ was introduced by spatially varied nanoapertures within the coupler as shown in the dotted box in Figure 1d. The generated LCGB, originated from two intersecting plane SPP beams with a rotational angle α, can be described as[47,60]

$$E_z(x, y) \propto \exp\left(\frac{-y^2}{W_0^2}\right)\cos[k_{SPP} y \sin(\alpha)] \tag{5}$$

where W_0 is the minimum of the beam waist of the incident light beam and the aperture radius of the coupler. The Gaussian distribution of the electric field would be modulated by a cosine function which depends on α so that the LCGB could propagate in a nondiffracting manner. The larger the rotational angle is, the more energy could be concentrated within the main lobe, and the propagation length is shorter. Therefore, the propagation characteristics of the generated LCGB can be controlled by properly setting the value of α. With such a phase-modulated coupler, a unidirectional LCGB could be generated according to the polarization state of the incident beam. Here, the uniform Λ-shaped nanoapertures within the compound AM-BS are modified to phase-modulated ones, so that the incident CPLG beam would be coupled to a nondiffracting LCGB instead of a planar SPP wave. The electric field distribution of the calculated normal component of the generated unidirectional LCGB with the incidence of LHCP is also shown in Figure 1d, which indicates better mode discrimination than that in Figure 1c.

All in all, our proposal is named as a compound phase-modulated AMBS (PM-AMBS) since it is a combination of grating structure and spatially varied Λ-shaped nanoapertures. With such PM-AMBS, the incident CPLG beam could be split into different directions according to the carried AM (both SAM and OAM).

SIMULATION RESULTS

To verify our proposal, finite-different time-domain (FDTD) simulations have been performed. The thickness of the gold film and the operation vacuum wavelength are set as 100 nm and λ = 980 nm (corresponding to $\lambda_{SPP} \approx$ 960 nm),

DOI: 10.1021/acsphotonics.9b01437
ACS Photonics XXXX, XXX, XXX−XXX

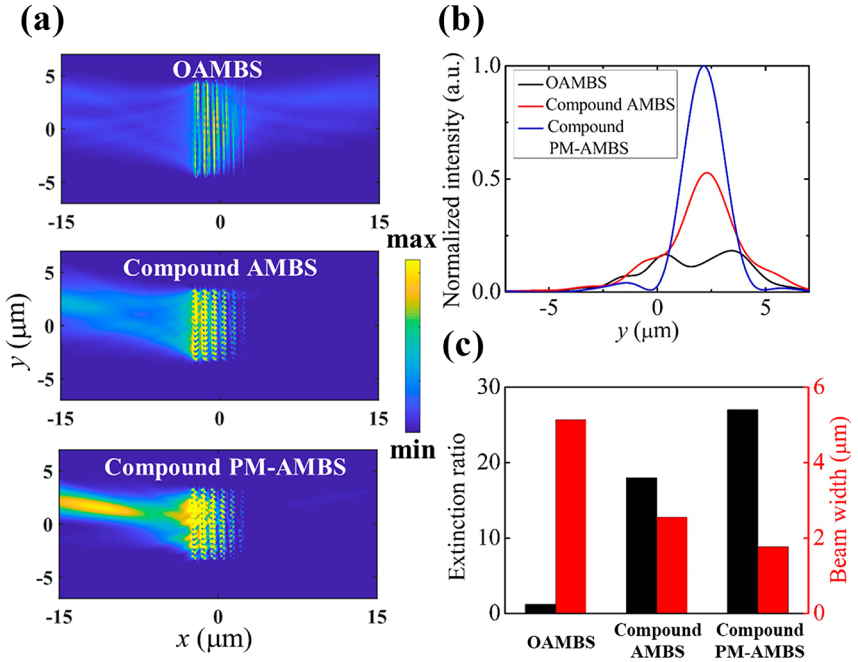

Figure 2. Comparisons of three beam splitters (OAMBS/compound AMBS/compound PM-AMBS) (a) Normalized intensity distribution of the launched SPP beam. (b) Intensity distribution curve of the launched SPP beam along the y-direction at $x = -15$ μm. (c) Simulated extinction ratio and beam width of the launched SPP beam at $x = -15$ μm.

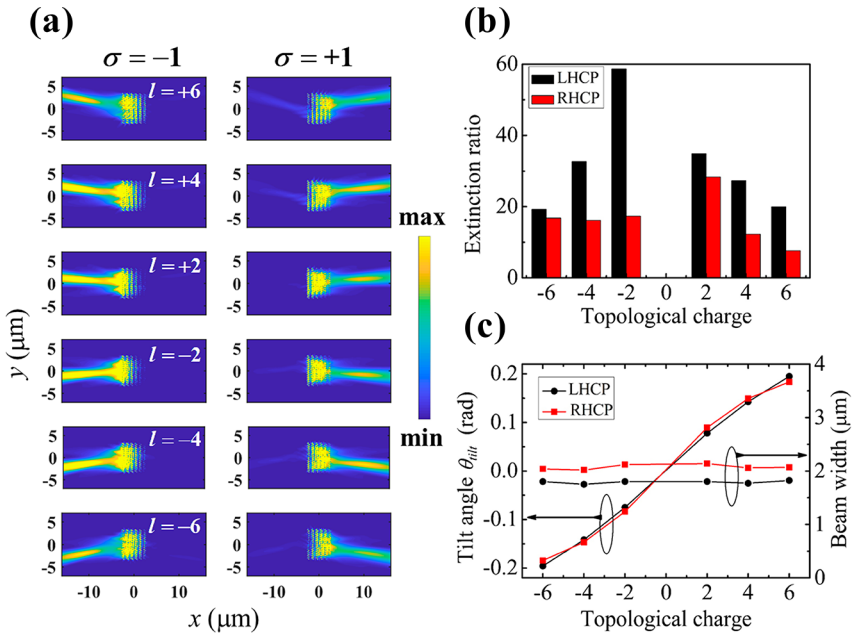

Figure 3. (a) Simulated intensity distributions of launched SPP beams for incident light beams carrying different AM. (b) Simulated extinction ratio vs topological charge of OAM modes for both LHCP and RHCP. (c) Simulated tilt angle θ_{tilt} and beam width at $|x| = 15$ μm of launched SPP beam vs topological charge.

respectively. The simulated length/width of the slit within the OAMBS is set as 9 μm/200 nm, while the corresponding geometric parameters for the compound PM-AMBS and compound AMBS are given in Figure 1c,d, respectively. The period of each beam splitter is set as one SPP wavelength of λ_{SPP}. In the simulation, the beam waist of the incident CPLG beam is set as 3 μm, and without loss of generality, the relative position is set as $r_0 = 5$ μm.

First, all three kinds of beam splitters have been simulated and compared. The simulated intensity distributions for OAMBS/compound AMBS/compound PM-AMBS with LHCP and a topological charge of 4 are shown in Figure 2a. For OAMBS, the launched SPP beams exist on both sides while only one side for the other two beam splitters. Furthermore, with phase modulation, the launched SPP beam would be much more concentrated. For clarity, the intensity distribution curves along the y-direction at $x = -15$ μm for all beam splitters are provided in Figure 2b. The peak intensity for compound PM-AMBS is almost twice that of compound AMBS without phase modulation. Besides, the

DOI: 10.1021/acsphotonics.9b01437
ACS Photonics XXXX, XXX, XXX−XXX

beam width at $x = -15$ μm (estimated from the Gaussian fitting of the intensity curve) is also shown in Figure 2c. Obviously, the launched SPP beam from compound PM-AMBS possesses the smallest beam width. Therefore, considering both coupling efficiency and beam width, the PM-AMBS would be most suitable for OAM beam splitting. Besides, Figure 2c shows the extinction ratio, which is defined as the ratio of transmission coefficients of the two sides. The higher the extinction ratio is, the better the mode discrimination of SAM. The Λ-shaped nanoapertures (including compound AMBS and PM-AMBS) could achieve polarization-controlled unidirectional launching of the SPP beam with an extinction ratio larger than 20. Notably, the extinction ratio can be further improved after phase modulation. Thus, the compound PM-AMBS also possesses optimal SAM mode discrimination. As expected, the compound PM-AMBS can achieve the best performance.

Next, the AM beam splitting performance of compound PM-AMBS is investigated in more detail. Figure 3a shows the simulated intensity distributions of the launched SPP beams for the different AM carried by the incident light beams. It can be seen that the launched SPP beams would propagate toward different directions according to the AM. Figure 3b shows the extinction ratio vs topological charge for both LHCP and RHCP. The extinction ratios for different AM modes are quite different. There are several factors to cause such a difference. First, the maximum extinction conditions of Λ-shaped nanoapertures only work well when no phase gradient exists along the coupler and the extinction condition would be worse as the phase gradient is larger. Therefore, the extinction ratio for the smaller phase gradient case ($l = 2$ and $l = -2$) would be relatively larger. Then, the SPP beam would be unidirectionally launched due to the near-field interference of the circular-polarized dipole.[48] The SPP beam launched from the RHCP incident beam would be preferred to the left, while to the right for the LHCP case when there is a positive phase gradient along the y-direction and vice versa. Therefore, for an LHCP incident beam, the extinction ratio for the negative topological charge is larger than that for the positive one, and for RHCP, it is opposite. Next, the asymmetric distribution of intensity exerted on the structure also leads to the different extinction ratio for the left and right side. Therefore, the extinction ratio for LHCP is larger than that for RHCP since much more intensity is incident on the left side of the structure. Finally, the relative position r_0 would also affect the extinction ratio dramatically (see Supporting Information for details). It should be mentioned that the minimum extinction ratio is larger than 8, which is high enough to render good SAM discrimination.

Figure 3c shows the tilt angle θ_{tilt} vs different AM carried by incident light beams. The tilt angle is nearly the same for LHCP and RHCP and would increase with the topological charge. Therefore, such a BS could be applied to separate OAM modes into different paths with different tilt angles. However, it should be noted that as the absolute value of the topological charge is larger, the tilt angle would increase slowly so that the ability of mode discrimination would be deteriorated. Therefore, the launched SPP beam with a smaller beam width is essential because the overlapping between two adjacent modes could be reduced. Figure 3c also shows the beam width at $|x| = 15$ μm vs different AM. The simulated beam width is about 1.8 μm/2.1 μm for LHCP/RHCP, and the small difference is mainly due to the asymmetry of intensity and phase distribution for the left and right sides. Besides, the corresponding comparison of beam width with compound AMBS without phase modulation is also given (see Supporting Information for details). Obviously, there would be a smaller beam width with phase modulation for all cases, which would be greatly helpful to improve the OAM mode discrimination. In addition, it should be mentioned that the proposed structure is not achromatic and could only operate within a limited wavelength range of several tens of nanometers around the designed wavelength (see Supporting Information for details).

All in all, with our proposed compound PM-AMBS, the incident CPLG beam could be separated into different paths on chip according to the carried AM (both SAM and OAM) with optimal mode discrimination.

EXPERIMENTAL RESULTS

Besides the numerical simulations, the corresponding experiments have also been carried out by fabricating several samples with a focused ion beam machine (FIB) (Tescan LYRA3). A 100-nm-thick gold film is evaporated on a quartz substrate with a 5-nm-thick buffer layer of titanium through vapor deposition. Figure 4a is the scanning electron microscope (SEM) image of the whole structure composed of the compound PM-AMBS and scattering gratings in both sides, and the enlarged area shows the details. Two gratings in each side scatter the generated SPP beams into free-space propagation modes for measurement, and the spacing between the two gratings is about 65 μm. For the measurement, a 980 nm laser source (Thorlabs, CLD1015) is illuminated followed by a polarizer and a quarter-wave plate (QWP). A spatial light modulator (PLUTO, NIR-015) is utilized to generate a spiral phase distribution. Then, a high numerical aperture objective (Nikon, NA = 0.9) is applied to generate a focused vortex beam with a beam waist of ~3 μm, and another objective (Nikon, NA = 0.3) is adopted to collect the scattered light. Last, the scattered

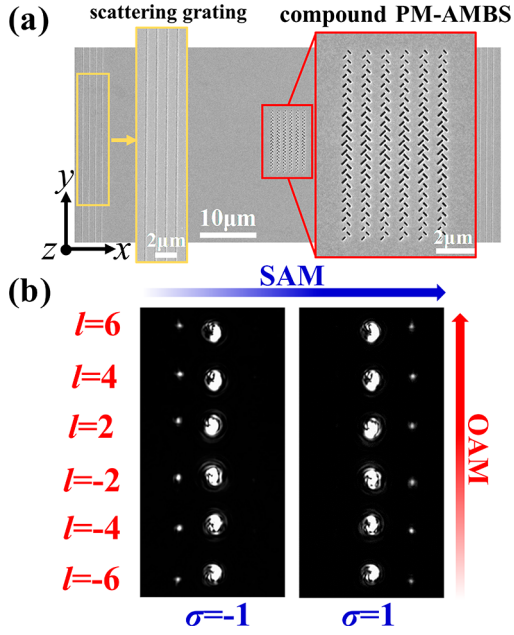

Figure 4. (a) SEM image of our proposed compound PM-AMBS in the middle and scattering gratings in both sides. The enlarged areas show the details. (b) Scattered signals of launched SPP beams for incident light beams carrying different AM.

DOI: 10.1021/acsphotonics.9b01437
ACS Photonics XXXX, XXX, XXX−XXX

light is detected by a charge-coupled device (CCD) camera (Thorlabs, 4070M-USB).

The typical measured results for incidence with different AM are shown in Figure 4b. The smaller bright spots are scattered light of the launched unidirectional SPP beams through the grating, while the larger one is that scattered by the beam splitter. Through the positions of those spots, it could be found that different incident modes have been separated into different paths according to the AM (l = −6, −4, −2, 2, 4, 6 and σ = −1, 1).

Furthermore, more information such as the transverse intensity distribution, the tilt angle, and the extinction ratio vs AM carried by the incident light beam could be obtained by carefully dealing with the measured spots. First, the measured intensity distribution curve of the launched SPP beam along the y-direction at $|x|$ = 30 μm for different AM is shown in Figure 5a, in which the intensity is normalized by the threshold

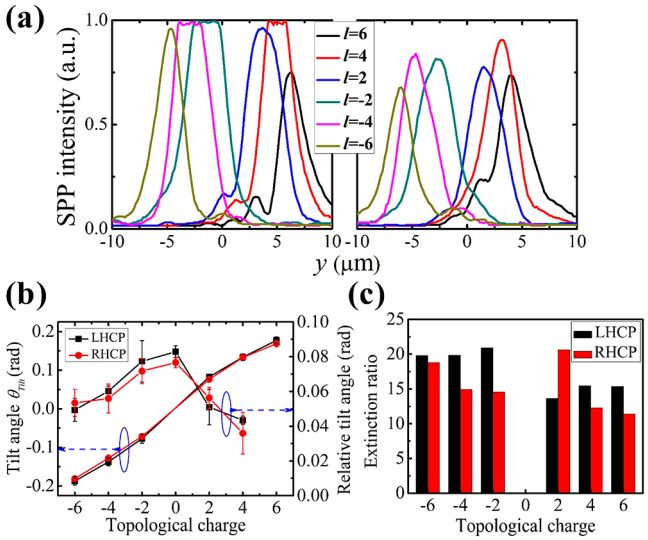

Figure 5. (a) Measured intensity distribution curve of the launched SPP beam along the y-direction at $|x|$ = 30 μm for different AM (left subgraph for LHCP and right for RHCP). (b) Measured tilt angle θ_{tilt} of launched SPP beam vs topological charge for both LHCP and RHCP. (c) Measured extinction ratio vs topological charge for both LHCP and RHCP.

of the CCD camera. The left part of Figure 5a corresponds to LHCP incidence, while the right part is for RHCP incidence. Typically, the exciting efficiency for LHCP is larger than that for RHCP due to the asymmetric intensity distribution of incident light beam as discussed in the Simulation Results. The difference of exciting efficiency is mainly induced by the different intensity distribution exerted on the device for different OAM modes since the relative ratio of different modes depends on the relative position of r_0 and the beam waist of the incident light beam. In the left case, the flat top of the intensity curve for l = −4, −2, and 4 results from the CCD saturation. From Figure 5a, it could be found that the different OAM modes have been separated into different positions in the transverse direction.

For clarity, the measured tilt angle θ_{tilt} of the launched SPP beam vs topological charge for both LHCP and RHCP is shown in Figure 5b. Similar to the simulation results, the tilt angle varies from $\theta_{tilt} \approx -0.18$ rad to $\theta_{tilt} \approx 0.17$ rad as the topological charge varies from l = −6 to l = 6. And only a little difference between the results of two circular polarization states is observed. Actually, the result is much closer to the case with relative position r_0 = 5.5 μm in simulation (see Supporting Information for details). Besides, the relative tilt angle is defined as the difference value between the tilt angles of adjacent modes. It could be found that the relative angle would be reduced for a larger absolute value of topological charge, which is consistent with the simulation results. The smallest relative tilt angle of about 0.036 rad in our case occurs when l = −6 for LHCP, which equals a transverse position interval of about 1.1 μm. Figure 5c shows the measured extinction ratio vs topological for both LHCP and RHCP, and the values for all cases are larger than 10. This indicates that the proposed device could separate different SAM beams successfully. Compared to the simulated extinction ratio, there is a little difference. One reason is that in the experiment the focal spot of the incident beam is not perfectly "donut" shaped due to the alignment error, which leads to a tiny difference between the experimental and the simulation results. Besides, the calculation of the extinction ratio in measurement is a little different from that in simulation (see Supporting Information for details). The efficiency of the device is estimated by the power of the incident beam over that of the scattered light, and the value is about −34.25 dB (see Supporting Information for details).

DISCUSSION AND CONCLUSION

In conclusion, we have proposed and demonstrated a phase-modulated AM beam splitter that could separate AM modes into different directions. The device is implemented along the azimuth direction of the incident light beam profile, comprising a group of phase-modulated SAM beam splitters with a measured extinction ratio larger than 10. Through such phase modulation, the nondiffracting LCGB could be generated, and thus the mode discrimination could be significantly improved. The measured spatial interval for OAM mode splitting is larger than 1.1 μm at a detection position of 30 μm (with a topological charge interval of 2). To further improve the mode discrimination, there are two possible solutions for increasing the spatial interval of two adjacent separated modes or reducing the beam width of the generated LCGB. Intuitively, the spatial interval is proportional to the product of the tilt angle and the detection distance. First, the tilt angle can be further enlarged by reducing the beam waist of the incident beam as the phase gradient is increased. However, there would be a trade-off between the tilt angle and the SPP beam width (see Supporting Information for details). Second, increasing the detection distance would also introduce larger beam divergence. Therefore, the mode discrimination would be limited by the beam width by enlarging either the tilt angle or the detection distance. Interestingly, it is hopeful to further shrink the beam width of the generated LCGB by introducing additional phase modulation, which could be achieved by designing the geometrical shape of the upper dielectric layer.[69] Therefore, with proper beam waist of incidence and detecting position, accompanied by an additional beam compression, the mode discrimination could be further improved. All in all, an AM beam splitter is achieved, and we believe that our proposal is very promising to achieve a highly compact photonic integrated circuit.

DOI: 10.1021/acsphotonics.9b01437
ACS Photonics XXXX, XXX, XXX−XXX

■ ASSOCIATED CONTENT

Supporting Information

The Supporting Information is available free of charge at https://pubs.acs.org/doi/10.1021/acsphotonics.9b01437.

Comparison of extinction ratios for different relative positions, comparison of beam widths and peak intensities between compound AMBS and PM-AMBS, tilt angles and beam widths for different relative positions, comparison of extinction ratios between simulation and measurement, comparison of tilt angles and beam widths for incident light beams with different beam waists, coupling efficiency, and operation bandwidth (PDF)

■ AUTHOR INFORMATION

Corresponding Author

*E-mail: x-feng@tsinghua.edu.cn.

ORCID

Xue Feng: 0000-0002-9057-1549

Wei Zhang: 0000-0002-6848-6807

Author Contributions

X.Z. and X.F. developed the theory. X.Z. ran the numerical simulations and did the experiments. X.Z. and X.F. wrote the paper. K.C., F.L., and W.Z. provided useful discussions. Y.H. revised the manuscript. All authors read and approved the manuscript.

Notes

The authors declare no competing financial interest.

■ ACKNOWLEDGMENTS

This work was supported by the National Key Research and Development Program of China (2018YFB2200402, 2017YFA0303700), the National Natural Science Foundation of China (Grant Nos. 61875101 and 61621064), Beijing Innovation Center for Future Chip, and Beijing Academy of Quantum Information Science. The authors would like to thank Peng Zhao, Jiayi Ouyang, and Tuo Qu for their valuable discussions and helpful comments. Most of all, I want to thank Tian Bian very much for prettifying the illustrations.

■ REFERENCES

(1) Bialynicki-Birula, I.; Bialynicka-Birula, Z. Canonical Separation of Angular Momentum of Light into Its Orbital and Spin Parts. *J. Opt.* **2011**, *13* (6), 064014.

(2) Barnett, S. M.; Allen, L.; Cameron, R. P.; Gilson, C. R.; Padgett, M. J.; Speirits, F. C.; Yao, A. M. On the Natures of the Spin and Orbital Parts of Optical Angular Momentum. *J. Opt.* **2016**, *18* (6), 064004.

(3) Crimin, F.; Mackinnon, N.; Götte, J.; Barnett, S. Optical Helicity and Chirality: Conservation and Sources. *Appl. Sci.* **2019**, *9* (5), 828.

(4) Bliokh, K. Y.; Rodríguez-Fortuño, F. J.; Nori, F.; Zayats, A. V. Spin−Orbit Interactions of Light. *Nat. Photonics* **2015**, *9* (12), 796−808.

(5) Allen, L.; Beijersbergen, M. W.; Spreeuw, R. J. C.; Woerdman, J. P. Orbital Angular Momentum of Light and the Transformation of Laguerre-Gaussian Laser Modes. *Phys. Rev. A: At., Mol., Opt. Phys.* **1992**, *45* (11), 8185−8189.

(6) Tan, H.; Deng, J.; Zhao, R.; Wu, X.; Li, G.; Huang, L.; Liu, J.; Cai, X. A Free-Space Orbital Angular Momentum Multiplexing Communication System Based on a Metasurface. *Laser Photonics Rev.* **2019**, 1800278.

(7) Djordjevic, I. B. Deep-Space and near-Earth Optical Communications by Coded Orbital Angular Momentum (OAM) Modulation. *Opt. Express* **2011**, *19* (15), 14277.

(8) Djordjevic, I. B.; Arabaci, M. LDPC-Coded Orbital Angular Momentum (OAM) Modulation for Free-Space Optical Communication. *Opt. Express* **2010**, *18* (24), 24722.

(9) Ren, H.; Li, X.; Zhang, Q.; Gu, M. On-Chip Noninterference Angular Momentum Multiplexing of Broadband Light. *Science* **2016**, *352* (6287), 805−809.

(10) Liu, J.; Li, S.; Ding, Y.; Chen, S.; Du, C.; Mo, Q.; Morioka, T.; Yvind, K.; Oxenløwe, L. K.; Yu, S.; et al. Orbital Angular Momentum Modes Emission from a Silicon Photonic Integrated Device for Km-Scale Data-Carrying Fiber Transmission. *Opt. Express* **2018**, *26* (12), 15471.

(11) Wang, J.; Yang, J.-Y.; Fazal, I. M.; Ahmed, N.; Yan, Y.; Huang, H.; Ren, Y.; Yue, Y.; Dolinar, S.; Tur, M.; et al. Terabit Free-Space Data Transmission Employing Orbital Angular Momentum Multiplexing. *Nat. Photonics* **2012**, *6* (7), 488−496.

(12) Bozinovic, N.; Yue, Y.; Ren, Y.; Tur, M.; Kristensen, P.; Huang, H.; Willner, A. E.; Ramachandran, S. Terabit-Scale Orbital Angular Momentum Mode Division Multiplexing in Fibers. *Science* **2013**, *340* (6140), 1545−1548.

(13) Cvijetic, N.; Milione, G.; Ip, E.; Wang, T. Detecting Lateral Motion Using Light's Orbital Angular Momentum. *Sci. Rep.* **2015**, *5* (1), 15422.

(14) Gorodetski, Y.; Shitrit, N.; Bretner, I.; Kleiner, V.; Hasman, E. Observation of Optical Spin Symmetry Breaking in Nanoapertures. *Nano Lett.* **2009**, *9* (8), 3016−3019.

(15) Fürhapter, S.; Jesacher, A.; Bernet, S.; Ritsch-Marte, M. Spiral Phase Contrast Imaging in Microscopy. *Opt. Express* **2005**, *13* (3), 689.

(16) Nicolas, A.; Veissier, L.; Giner, L.; Giacobino, E.; Maxein, D.; Laurat, J. A Quantum Memory for Orbital Angular Momentum Photonic Qubits. *Nat. Photonics* **2014**, *8* (3), 234−238.

(17) Nagali, E.; Sansoni, L.; Sciarrino, F.; De Martini, F.; Marrucci, L.; Piccirillo, B.; Karimi, E.; Santamato, E. Optimal Quantum Cloning of Orbital Angular Momentum Photon Qubits through Hong−Ou−Mandel Coalescence. *Nat. Photonics* **2009**, *3* (12), 720−723.

(18) Erhard, M.; Fickler, R.; Krenn, M.; Zeilinger, A. Twisted Photons: New Quantum Perspectives in High Dimensions. *Light: Sci. Appl.* **2018**, *7* (3), 17146−17146.

(19) Ambrosio, A.; Marrucci, L.; Borbone, F.; Roviello, A.; Maddalena, P. Light-Induced Spiral Mass Transport in Azo-Polymer Films under Vortex-Beam Illumination. *Nat. Commun.* **2012**, *3* (1), 989.

(20) Kuga, T.; Torii, Y.; Shiokawa, N.; Hirano, T.; Shimizu, Y.; Sasada, H. Novel Optical Trap of Atoms with a Doughnut Beam. *Phys. Rev. Lett.* **1997**, *78* (25), 4713−4716.

(21) Tsai, W.-Y.; Huang, J.-S.; Huang, C.-B. Selective Trapping or Rotation of Isotropic Dielectric Microparticles by Optical Near Field in a Plasmonic Archimedes Spiral. *Nano Lett.* **2014**, *14* (2), 547−552.

(22) Ng, J.; Lin, Z.; Chan, C. T. Theory of Optical Trapping by an Optical Vortex Beam. *Phys. Rev. Lett.* **2010**, *104* (10), 103601.

(23) Padgett, M.; Bowman, R. Tweezers with a Twist. *Nat. Photonics* **2011**, *5* (6), 343−348.

(24) Huang, H.; Xie, G.; Yan, Y.; Ahmed, N.; Ren, Y.; Yue, Y.; Rogawski, D.; Willner, M. J.; Erkmen, B. I.; Birnbaum, K. M.; et al. 100 Tbit/s Free-Space Data Link Enabled by Three-Dimensional Multiplexing of Orbital Angular Momentum, Polarization, and Wavelength. *Opt. Lett.* **2014**, *39* (2), 197.

(25) Ren, Y.; Xie, G.; Huang, H.; Li, L.; Ahmed, N.; Yan, Y.; Lavery, M. P. J.; Bock, R.; Tur, M.; Neifeld, M. A.; et al. Turbulence Compensation of an Orbital Angular Momentum and Polarization-Multiplexed Link Using a Data-Carrying Beacon on a Separate Wavelength. *Opt. Lett.* **2015**, *40* (10), 2249.

(26) Wang, X.-L.; Cai, X.-D.; Su, Z.-E.; Chen, M.-C.; Wu, D.; Li, L.; Liu, N.-L.; Lu, C.-Y.; Pan, J.-W. Quantum Teleportation of Multiple Degrees of Freedom of a Single Photon. *Nature* **2015**, *518* (7540), 516−519.

DOI: 10.1021/acsphotonics.9b01437
ACS Photonics XXXX, XXX, XXX−XXX

(27) Yue, Z.; Ren, H.; Wei, S.; Lin, J.; Gu, M. Angular-Momentum Nanometrology in an Ultrathin Plasmonic Topological Insulator Film. *Nat. Commun.* **2018**, *9* (1), 4413.
(28) Wu, P. C.; Tsai, W.-Y.; Chen, W. T.; Huang, Y.-W.; Chen, T.-Y.; Chen, J.-W.; Liao, C. Y.; Chu, C. H.; Sun, G.; Tsai, D. P. Versatile Polarization Generation with an Aluminum Plasmonic Metasurface. *Nano Lett.* **2017**, *17* (1), 445−452.
(29) Almeida, E.; Shalem, G.; Prior, Y. Subwavelength Nonlinear Phase Control and Anomalous Phase Matching in Plasmonic Metasurfaces. *Nat. Commun.* **2016**, *7* (1), DOI: 10.1038/ncomms10367.
(30) Chong, K. E.; Staude, I.; James, A.; Dominguez, J.; Liu, S.; Campione, S.; Subramania, G. S.; Luk, T. S.; Decker, M.; Neshev, D. N.; et al. Polarization-Independent Silicon Metadevices for Efficient Optical Wavefront Control. *Nano Lett.* **2015**, *15* (8), 5369−5374.
(31) Wang, L.; Kruk, S.; Koshelev, K.; Kravchenko, I.; Luther-Davies, B.; Kivshar, Y. Nonlinear Wavefront Control with All-Dielectric Metasurfaces. *Nano Lett.* **2018**, *18* (6), 3978−3984.
(32) Khorasaninejad, M.; Chen, W. T.; Devlin, R. C.; Oh, J.; Zhu, A. Y.; Capasso, F. Metalenses at Visible Wavelengths: Diffraction-Limited Focusing and Subwavelength Resolution Imaging. *Science* **2016**, *352* (6290), 1190−1194.
(33) Shalaev, M. I.; Sun, J.; Tsukernik, A.; Pandey, A.; Nikolskiy, K.; Litchinitser, N. M. High-Efficiency All-Dielectric Metasurfaces for Ultracompact Beam Manipulation in Transmission Mode. *Nano Lett.* **2015**, *15* (9), 6261−6266.
(34) Arbabi, A.; Horie, Y.; Bagheri, M.; Faraon, A. Dielectric Metasurfaces for Complete Control of Phase and Polarization with Subwavelength Spatial Resolution and High Transmission. *Nat. Nanotechnol.* **2015**, *10* (11), 937−943.
(35) Wang, S.; Wu, P. C.; Su, V.-C.; Lai, Y.-C.; Chen, M.-K.; Kuo, H. Y.; Chen, B. H.; Chen, Y. H.; Huang, T.-T.; Wang, J.-H.; et al. A Broadband Achromatic Metalens in the Visible. *Nat. Nanotechnol.* **2018**, *13* (3), 227−232.
(36) Andress, W. F.; Yoon, H.; Yeung, K. Y. M.; Qin, L.; West, K.; Pfeiffer, L.; Ham, D. Ultra-Subwavelength Two-Dimensional Plasmonic Circuits. *Nano Lett.* **2012**, *12* (5), 2272−2277.
(37) Gramotnev, D. K.; Bozhevolnyi, S. I. Plasmonics beyond the Diffraction Limit. *Nat. Photonics* **2010**, *4* (2), 83−91.
(38) Haffner, C.; Chelladurai, D.; Fedoryshyn, Y.; Josten, A.; Baeuerle, B.; Heni, W.; Watanabe, T.; Cui, T.; Cheng, B.; Saha, S.; et al. Low-Loss Plasmon-Assisted Electro-Optic Modulator. *Nature* **2018**, *556* (7702), 483−486.
(39) Ayata, M.; Fedoryshyn, Y.; Heni, W.; Baeuerle, B.; Josten, A.; Zahner, M.; Koch, U.; Salamin, Y.; Hoessbacher, C.; Haffner, C. High-Speed Plasmonic Modulator in a Single Metal Layer. *Science* **2017**, *358* (6363), 630−632.
(40) Barnes, W. L.; Dereux, A.; Ebbesen, T. W. Surface Plasmon Subwavelength Optics. *Nature* **2003**, *424* (6950), 824.
(41) Ozbay, E. Plasmonics: Merging Photonics and Electronics at Nanoscale Dimensions. *Science* **2006**, *311* (5758), 189−193.
(42) Mueller, J. P. B.; Leosson, K.; Capasso, F. Polarization-Selective Coupling to Long-Range Surface Plasmon Polariton Waveguides. *Nano Lett.* **2014**, *14* (10), 5524−5527.
(43) Lin, J.; Mueller, J. P. B.; Wang, Q.; Yuan, G.; Antoniou, N.; Yuan, X.-C.; Capasso, F. Polarization-Controlled Tunable Directional Coupling of Surface Plasmon Polaritons. *Science* **2013**, *340* (6130), 331−334.
(44) Lee, S.-Y.; Kim, K.; Kim, S.-J.; Park, H.; Kim, K.-Y.; Lee, B. Plasmonic Meta-Slit: Shaping and Controlling near-Field Focus. *Optica* **2015**, *2* (1), 6.
(45) Yin, X.; Chen, L.; Li, X. Polarization-Controlled Generation of Airy Plasmons. *Opt. Express* **2018**, *26* (18), 23251.
(46) Miroshnichenko, A. E.; Kivshar, Y. S. Polarization Traffic Control for Surface Plasmons. *Science* **2013**, *340* (6130), 283−284.
(47) Zhao, X.; Feng, X.; Zhao, P.; Liu, F.; Cui, K.; Zhang, W.; Huang, Y. Polarization-Controllably Launching Localized Cosine-Gauss Beam with Spatially Varied Metallic Nano-Apertures. *Opt. Express* **2019**, *27* (16), 22053.
(48) Rodriguez-Fortuno, F. J.; Marino, G.; Ginzburg, P.; O'Connor, D.; Martinez, A.; Wurtz, G. A.; Zayats, A. V. Near-Field Interference for the Unidirectional Excitation of Electromagnetic Guided Modes. *Science* **2013**, *340* (6130), 328−330.
(49) Huang, L.; Chen, X.; Bai, B.; Tan, Q.; Jin, G.; Zentgraf, T.; Zhang, S. Helicity Dependent Directional Surface Plasmon Polariton Excitation Using a Metasurface with Interfacial Phase Discontinuity. *Light: Sci. Appl.* **2013**, *2* (3), e70−e70.
(50) Ding, F.; Deshpande, R.; Bozhevolnyi, S. I. Bifunctional Gap-Plasmon Metasurfaces for Visible Light: Polarization-Controlled Unidirectional Surface Plasmon Excitation and Beam Steering at Normal Incidence. *Light: Sci. Appl.* **2018**, *7* (4), 17178−17178.
(51) Chen, J.; Chen, X.; Li, T.; Zhu, S. On-Chip Detection of Orbital Angular Momentum Beam by Plasmonic Nanogratings. *Laser & Photonics Reviews* **2018**, *12* (8), 1700331.
(52) Mei, S.; Huang, K.; Liu, H.; Qin, F.; Mehmood, M. Q.; Xu, Z.; Hong, M.; Zhang, D.; Teng, J.; Danner, A.; et al. On-Chip Discrimination of Orbital Angular Momentum of Light with Plasmonic Nanoslits. *Nanoscale* **2016**, *8* (4), 2227−2233.
(53) Epstein, I.; Lilach, Y.; Arie, A. Shaping Plasmonic Light Beams with Near-Field Plasmonic Holograms. *J. Opt. Soc. Am. B* **2014**, *31* (7), 1642.
(54) Gazzola, E.; Ruffato, G.; Romanato, F. Propagation of Grating-Coupled Surface Plasmon Polaritons and Cosine−Gauss Beam Generation. *J. Opt. Soc. Am. B* **2015**, *32* (8), 1564.
(55) Qiu, P.; Lv, T.; Zhang, Y.; Yu, B.; Lian, J.; Jing, M.; Zhang, D. Polarization Controllable Device for Simultaneous Generation of Surface Plasmon Polariton Bessel-Like Beams and Bottle Beams. *Nanomaterials* **2018**, *8* (12), 975.
(56) Epstein, I.; Remez, R.; Tsur, Y.; Arie, A. Generation of Intensity-Controlled Two-Dimensional Shape-Preserving Beams in Plasmonic Lossy Media. *Optica* **2016**, *3* (1), 15.
(57) He, X.; Ning, T.; Li, R.; Pei, L.; Zheng, J.; Li, J. Dynamical Manipulation of Cosine-Gauss Beams in a Graphene Plasmonic Waveguide. *Opt. Express* **2017**, *25* (12), 13923.
(58) Qiu, P.; Zhang, D.; Jing, M.; Lu, T.; Yu, B.; Zhan, Q.; Zhuang, S. Dynamic Tailoring of Surface Plasmon Polaritons through Incident Angle Modulation. *Opt. Express* **2018**, *26* (8), 9772.
(59) Xiao, K.; Wei, S.; Min, C.; Yuan, G.; Zhu, S. W.; Lei, T.; Yuan, X.-C. Dynamic Cosine-Gauss Plasmonic Beam through Phase Control. *Opt. Express* **2014**, *22* (11), 13541.
(60) Lin, J.; Dellinger, J.; Genevet, P.; Cluzel, B.; de Fornel, F.; Capasso, F. Cosine-Gauss Plasmon Beam: A Localized Long-Range Nondiffracting Surface Wave. *Phys. Rev. Lett.* **2012**, *109* (9), DOI: 10.1103/PhysRevLett.109.093904.
(61) Zhu, L.; Li, Y.; Sun, A.; Xiong, Z.; Liu, C.; Kong, Y.; Wang, S. Active-Polarization-Controlled Long-Depth Focus Generated by Orthogonal Nanoslit Array. *Appl. Phys. Express* **2016**, *9* (8), 082201.
(62) Avayu, O.; Epstein, I.; Eizner, E.; Ellenbogen, T. Polarization Controlled Coupling and Shaping of Surface Plasmon Polaritons by Nanoantenna Arrays. *Opt. Lett.* **2015**, *40* (7), 1520.
(63) Schley, R.; Kaminer, I.; Greenfield, E.; Bekenstein, R.; Lumer, Y.; Segev, M. Loss-Proof Self-Accelerating Beams and Their Use in Non-Paraxial Manipulation of Particles' Trajectories. *Nat. Commun.* **2014**, *5* (1), DOI: 10.1038/ncomms6189.
(64) Minovich, A.; Klein, A. E.; Janunts, N.; Pertsch, T.; Neshev, D. N.; Kivshar, Y. S. Generation and Near-Field Imaging of Airy Surface Plasmons. *Phys. Rev. Lett.* **2011**, *107* (11), DOI: 10.1103/PhysRevLett.107.116802.
(65) Minovich, A. E.; Klein, A. E.; Neshev, D. N.; Pertsch, T.; Kivshar, Y. S.; Christodoulides, D. N. Airy Plasmons: Non-Diffracting Optical Surface Waves: Airy Plasmons. *Laser & Photonics Reviews* **2014**, *8* (2), 221−232.
(66) Genevet, P.; Dellinger, J.; Blanchard, R.; She, A.; Petit, M.; Cluzel, B.; Kats, M. A.; de Fornel, F.; Capasso, F. Generation of Two-Dimensional Plasmonic Bottle Beams. *Opt. Express* **2013**, *21* (8), 10295.
(67) Epstein, I.; Arie, A. Dynamic Generation of Plasmonic Bottle-Beams with Controlled Shape. *Opt. Lett.* **2014**, *39* (11), 3165.

DOI: 10.1021/acsphotonics.9b01437
ACS Photonics XXXX, XXX, XXX−XXX

(68) Epstein, I.; Arie, A. Arbitrary Bending Plasmonic Light Waves. *Phys. Rev. Lett.* **2014**, *112* (2), DOI: 10.1103/PhysRevLett.112.023903.
(69) Garcia-Ortiz, C. E.; Cortes, R.; Gómez-Correa, J. E.; Pisano, E.; Fiutowski, J.; Garcia-Ortiz, D. A.; Ruiz-Cortes, V.; Rubahn, H.-G.; Coello, V. Plasmonic Metasurface Luneburg Lens. *Photonics Res.* **2019**, 7 (10), 1112.

DOI: 10.1021/acsphotonics.9b01437
ACS Photonics XXXX, XXX, XXX−XXX